Chemical Science

Accepted Manuscript

This article can be cited before page numbers have been issued, to do this please use: K. Yuhara, S. Takemori, T. Yanagihara, S. Ohtani, T. Ogoshi and K. Tanaka, *Chem. Sci.*, 2026, DOI: 10.1039/D5SC08753H.

ROYAL SOCIETY OF CHEMISTRY

rsc.li/chemical-science

View Article Online
DOI: 10.1039/D5SC08753H

Guest-Induced Emission Enhancement in the Permanent Porous Conjugated Carboracycle Crystal

Kazuhiro Yuhara,[a] Sota Takemori,[a] Takumi Yanagihara,[a] Shunsuke Ohtani,[b] Tomoki Ogoshi,[b,c] Kazuo Tanaka*[a,d]

[a] Department of Polymer Chemistry, Graduate School of Engineering, Kyoto University, Katsura, Nishikyo-ku, Kyoto 615–8510, Japan

[b] Department of Synthetic Chemistry and Biological Chemistry, Graduate School of Engineering, Kyoto University, Katsura, Nishikyo-ku, Kyoto 615–8510, Japan

[c] WPI Nano Life Science Institute (WPI-NanoLSI), Kanazawa University, Kakuma-machi, Kanazawa, Ishikawa 920–1192, Japan

[d] Department of Technology and Ecology, Graduate School of Global Environmental Studies, Kyoto University, Katsura, Nishikyo-ku, Kyoto 615–8510, Japan

E-mail: tanaka@poly.synchem.kyoto-u.ac.jp

Abstract

Macrocyclization can provide available space for realizing host–guest-mediated molecular sensing based on the regulation of excited-state structural change. Here we report guest-induced luminescent changes in crystalline *o*-carborane-involved conjugated macrocycles where intrinsic porous crystal is developed with 1D channels. The crystal can capture C4-length vaporous guests and subsequently exhibit guest-induced emission enhancement through the suppression of excited-state structural relaxation. Notably, the crystal showed successful reversible guest encapsulation without losing its crystalline porosity and heat resistance up to 500 °C.

Introduction

Solid-state emissive molecules with stimuli-responsiveness have attracted tremendous attention as a platform for next-generation optoelectronics.[1] However, environmental sensitivity is often spoiled in conventional organic luminophores due to aggregation-caused quenching (ACQ). As one of the potential strategies for overcoming the ACQ problem, the employment of aggregation-induced emission (AIE)-active molecules (AIEgens), which can show intense emission only in solid states, is valid because they intrinsically have environment-sensitive optical properties.[2] Previous reports have

View Article Online
DOI: 10.1039/D5SC08753H

suggested that solid-state luminescent properties in AIE should be related with the degree of structural relaxation in the excited state.[3,4] When surrounding molecules tightly restrict molecular motions of chromophores in the excited state, the photochemical channels to non-radiative deactivation processes should be closed, followed by significant emission enhancement.[5] Based on this mechanism, various AIEgens have been extensively studied on their structure–property relationships and applied as imaging probes.[6] Currently, further applications in the next-generation smart devices are explored, and solid-state emissive materials including AIEgens are expected to have more stimuli-responsiveness i.e. luminochromic properties in response to external stimuli or environmental changes.[7] As a next research step, it would be of importance to design external stimuli to control the solid-state luminescence. Restriction of molecular motions by aggregation often hinders responses to surrounding environments, followed by decreasing their stimuli-responsiveness and loosing controllability of luminescent properties.[8] A promising design strategy to enhance sensitivity toward environmental changes is the introduction of spaces within the molecule. For example, macrocycle-containing AIEgens can provide an internal cavity that can accommodate molecular motion, and host–guest properties of macrocycles can be a trigger for controlling solid-state optical properties.[9] So far, many studies have reported AIEgen-based macrocycles,[10] whereas only a few reports have addressed solid-state host–guest properties and their effect on luminescence.

A boron and carbon cluster, *o*-carborane, has been known to work as a key unit for constructing functional AIEgens.[11] *C*-aryl *o*-carborane derivatives typically show intramolecular charge transfer (ICT) emission originating from orbital conjugation between the aryl moiety and the cluster unit (Figure 1a).[12] The excited-state structures in the ICT states were theoretically studied with the following two structural parameters: lengths of the carbon–carbon bond in the cluster (C_{cage}–C_{cage} bond) and dihedral angles between aryl units and the C_{cage}–C_{cage} bond ($\varphi_{Ar\text{-}CB}$). The ICT state can be formed when π-plane of the aryl moiety perpendicularly orients to the C_{cage}–C_{cage} bond ($\varphi_{Ar\text{-}CB} \sim 90°$), accompanied with significant elongation of the bond from 1.6–1.9 Å in the ground state to 2.2–2.4 Å in the excited state (Figure 1b left).[13] Furthermore, recent studies suggest that completely charge separated state, followed by the non-emissive dark state possessing only slight oscillator strength, should be formed, when the aryl moiety parallelly aligns to the C_{cage}–C_{cage} bond ($\varphi_{Ar\text{-}CB} \sim 0°$) accompanied with its further elongation

View Article Online
DOI: 10.1039/D5SC08753H

to ~2.5 Å (Figure 1b right).[14,15] These emissive ICT and non-emissive dark states competitively play key roles in photochemistry of *o*-carboranes. As a related example, we previously found that host–guest interaction can regulate excited-state structural relaxation in the *o*-carborane-based macrocycles containing pseudo-crown ether (Figure 1c).[16] The macrocycles showed emission enhancement upon solution-state host–guest complexation by the suppression of molecular motion that quenches emission.

There have been numbers of C_3-symmetric macrocyclic compounds with precise host–guest chemistry.[17,18] *C*,*C*′-difunctionalized *o*-carborane can be implemented into the corner of molecular triangles.[19] Herein, we report the macrocycle consisting of cyclo-trimerized diphenyl *o*-carborane (**CB3Ph6**, Figure 1d) as a conjugated type of carboracycle.[20] Interestingly, **CB3Ph6** formed permanent intrinsic porous crystal,[21] where guest-accessible 1D channels were developed through columnar stacking of the macrocycles. Moreover, **CB3Ph6** showed AIE properties, and its porous crystal showed emission enhancement upon encapsulation of vaporous guests. Theoretical calculation suggests that cavity-filling by guests should restrict the excited-state structural relaxation, leading to closing the channel to the non-emissive dark states. In addition, the crystal showed reversible guest release and capture without changing its crystalline porosity and no chemical decomposition up to 500 °C. This is the first example, to the best of our knowledge, to offer the porous crystal with the guest-encapsulation-triggered luminochromic behaviors and superior thermal stability based on the carboracycle molecule.

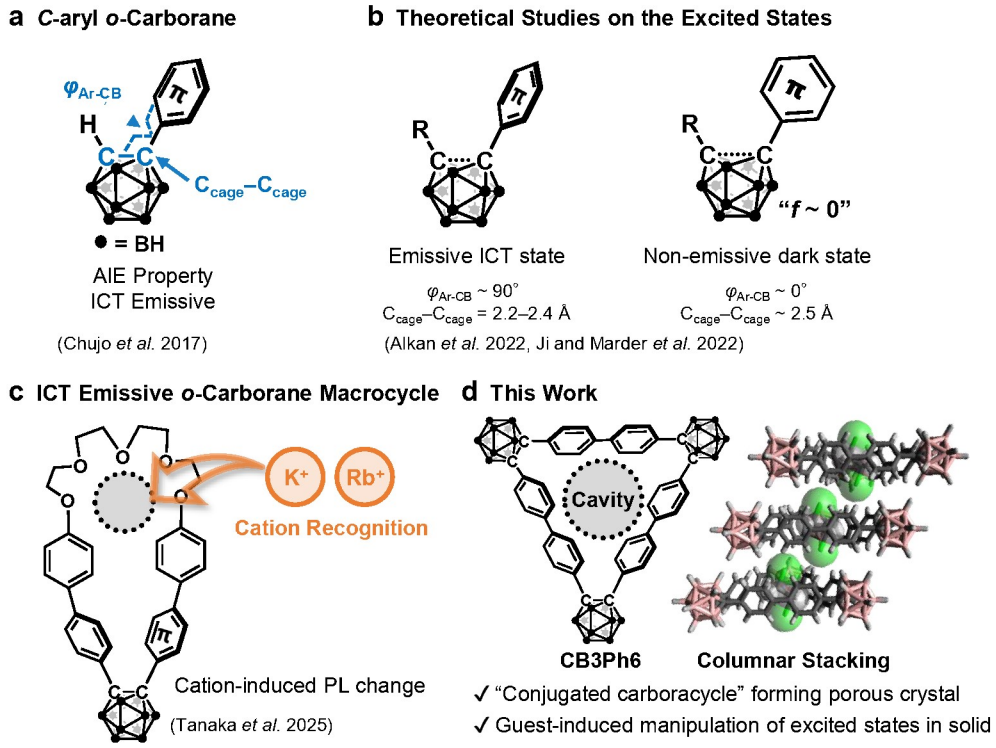

View Article Online
DOI: 10.1039/D5SC08753H

Figure 1. Reported examples of (a) *C*-aryl *o*-carborane derivatives, (b) theoretical studies on the excited states of the derivatives forming ICT states, and (c) ICT emissive *o*-carborane-based macrocycle. *f* denotes oscillator strength. (d) Chemical structure and crystal-state columnar stacking of **CB3Ph6** with the overview of this work.

Results and Discussion

Synthesis and crystallization

The macrocycle, **CB3Ph6**, was successfully synthesized by Ni(0)-mediated trimerization of 1,2-bis(4-bromophenyl)-*o*-carborane[22] (Schemes S1 and S2, Charts S1–S3 and S10). The dibrominated precursor was consumed quantitatively under the reaction condition. Purification was initially performed by column chromatography on SiO_2. After column chromatography, it was still a mixture of the product and other byproducts. Then recrystallization was performed with 1,2-dichloroethane (DCE) to afford pure crystalline products. The synthesis of the macrocycle proceeded in a poor isolated yield of 4% probably due to the formation of large amount of precipitation, likely an oligomerization or polymerization product. The single-crystal of **CB3Ph6** containing DCE (**DCE@CB3Ph6**) was obtained by vapor diffusion of MeOH into the DCE solution at −30 °C, followed by slow evaporation of solvent at room temperature. Single-crystal X-ray diffraction (SCXRD) analysis revealed that DCE molecules occupied the cavity of each macrocycle to form 1:1 host–guest complex (Figures 2ab and S1, Table S1). Encapsulated DCE molecules had multiple C–H···π interactions with biphenyl sides located between *o*-carborane corners. **CB3Ph6** molecules aligned in the columnar structure with 1D channels (Figure 2c). Stacked **CB3Ph6** molecules were involved in B–H···H–B and B–H···H–C contacts. Columns were assembled to form packed structure, where several B–H···B, B–H···H–B, and B–H···H–C contacts existed among them (Figure 2d).

View Article Online
DOI: 10.1039/D5SC08753H

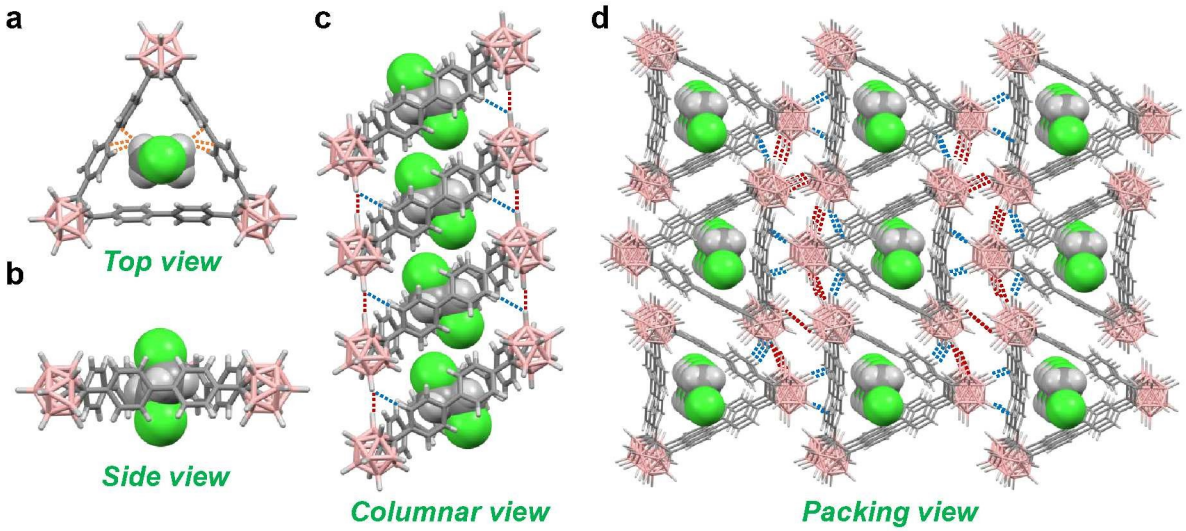

Figure 2. Single-crystal structures of **DCE@CB3Ph6**: (a) top, (b) side, (c) columnar, and (d) packing views. Orange, red and blue dotted lines indicate C–H···π, B–H···(H–)B, and B–H···H–C contacts (< sum of vdW radii), respectively. Colors: C, gray; B, pink; H, white; Cl, green.

Adsorption and thermal properties

To investigate the effects of solvent inclusion on physical properties, guest-free crystal (**CB3Ph6**α) was prepared by heating of **DCE@CB3Ph6** at 100 °C under vacuum for 3 h. The removal of DCE was monitored by ^{1}H NMR spectrum (Chart S4). Unfortunately, a single crystal sample of **CB3Ph6**α suitable for the SCXRD analysis was not able to be obtained. Then, the crystal structure of **CB3Ph6**α was examined by powder X-ray diffraction (PXRD) analysis (Figures S3 and S4). Initially, the PXRD peak positions of **CB3Ph6**α were almost consistent with **DCE@CB3Ph6**, suggesting that they should have similar molecular packing. Moreover, from the index assignment with PXRD patterns, it was revealed that **CB3Ph6**α has the same space group (*C*2/c) to **DCE@CB3Ph6** with only slight change in crystal lattice upon guest removal. These results indicate that crystalline molecular arrangement of **CB3Ph6**α can be preserved during the guest-removing process. From these facts, we presumed that **CB3Ph6**α might form unfilled channels where guest molecules can be accommodated. To examine validity of this assumption, N_2 adsorption isotherm of **CB3Ph6**α was collected (Figure 3a). It was found that **CB3Ph6**α had a typical type-I N_2 isotherm, indicating the presence of microporosity. The specific surface area was calculated as 1.5×10^2 $m^2 \cdot g^{-1}$ (Figure S8), which was on the same order of magnitude to a porous crystal based on triangle compounds.[18] These results indicate that **CB3Ph6**α has permanent intrinsic porosity and maintains crystalline molecular alignment even after removal of guest

View Article Online
DOI: 10.1039/D5SC08753H

molecules.[18] Furthermore, adsorption isotherms were collected for CO_2, methane (CH_4), ethane (C_2H_6), butane (C_4H_{10}), and *n*-hexane (C_6H_{14}) (Figure S9, Table 1). **CB3Ph6**α showed the highest adsorption capability on C_4H_{10}, which has multiple C–H moieties and the most similar molecular size to DCE among the tested gas. Therefore, C4-length guests should have the best size-matching to the cavity. Decrease in adsorption capacity on C_6H_{14} is possibly because of the size incompatibility leading to the ineffective formation of C–H···π contacts between host and guest molecules. Consequently, adsorption data suggest that **CB3Ph6**α can capture vaporous guests with C4-length via C–H···π interactions.

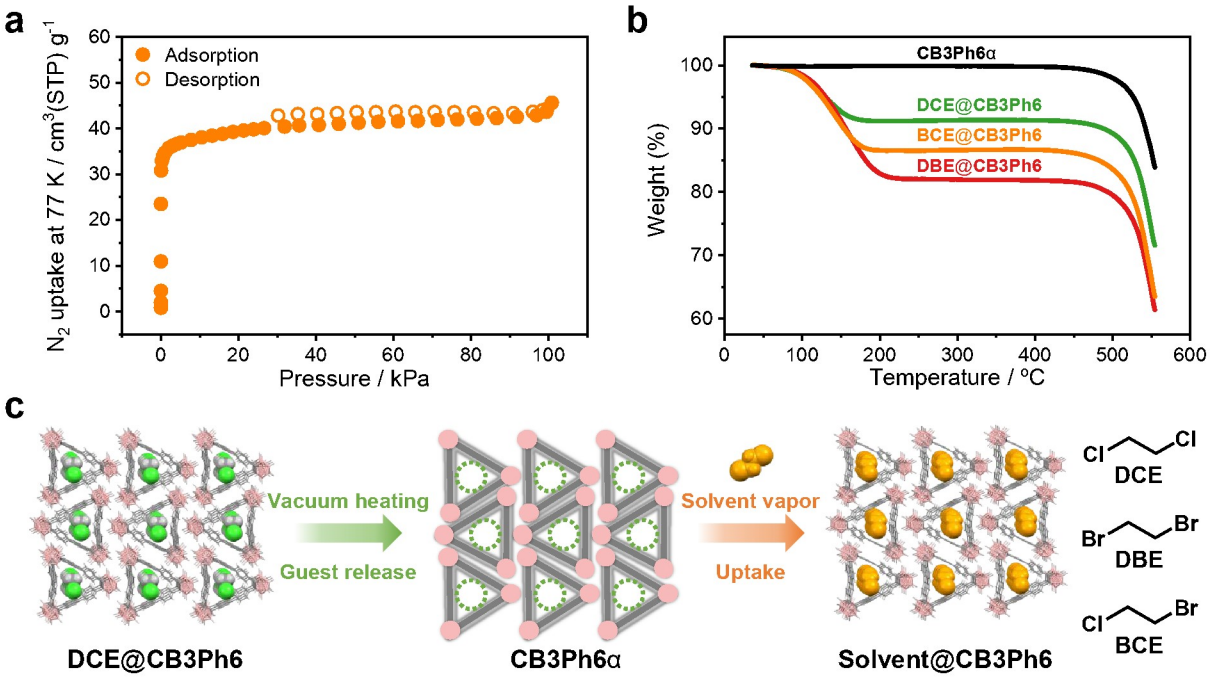

Figure 3. (a) N_2 sorption isotherm of **CB3Ph6**α recorded at 77 K. Solid and open circles represent adsorption and desorption, respectively. (b) TGA thermograms of **CB3Ph6**α (black), **DCE@CB3Ph6** (green), **DBE@CB3Ph6** (red), and **BCE@CB3Ph6** (orange). (c) Representation of guest removal and encapsulation processes. Molecular packing of **CB3Ph6**α was depicted in detail as far as experimentally revealed. Gray rods and pink filled circles, and green dotted circles represent biphenyl and *o*-carborane units, and vacant channels, respectively.

Table 1. Summary of the adsorption capacities of **CB3Ph6**α

Adsorbate	V / cm^3(STP)g^{-1} at 298 K
CO_2	22.8 [a]
CH_4	10.8 [a]
C_2H_6	25.2 [a]

View Article Online
DOI: 10.1039/D5SC08753H

C_4H_{10}	27.3 [a]
C_6H_{14}	19.8 [b]

[a] Measured under 100.4 kPa. [b] Measured under 18.3 kPa (saturated).

Guest encapsulation of **CB3Ph6**α was studied by solid-vapor adsorption experiments. The crystalline sample of **CB3Ph6**α was exposed to the vapor of 1,2-dibromoethane (DBE) or 1-bromo-2-chloroethane (BCE), which have the similar molecular size to DCE, to prepare guest-loaded crystals (**DBE@CB3Ph6** or **BCE@CB3Ph6**, respectively). ^{1}H NMR spectra indicated that 1:1 encapsulation of the solvent molecules proceeded in both **CB3Ph6** (Charts S5 and S6, Table S2). PXRD patterns of **DBE@CB3Ph6** and **BCE@CB3Ph6** were almost identical to those of **DCE@CB3Ph6** and **CB3Ph6**α (Figure S4), indicating that crystal-state arrangement of **CB3Ph6** should be hardly changed upon adsorption of DBE or BCE. Re-uptake of DCE on **CB3Ph6**α was also monitored by PXRD and ^{1}H NMR measurements (Figure S5, Chart S7). The resulting crystals were evaluated with thermogravimetric analysis (TGA) (Figures 3b and S10). Accordingly, the solvated crystals showed 10–20% weight loss between 100–200 °C assignable to solvent release. Molar ratio of included solvents to **CB3Ph6** was calculated as 1:1 in three solvated crystals as observed in ^{1}H NMR spectra (Table S2). The solvent release was also confirmed by endothermic peaks in differential scanning calorimetry thermograms (Figure S11). In contrast, **CB3Ph6**α hardly showed weight loss within 100–200 °C, indicating complete removal of the guest solvents during activation. Reported porous organic compounds typically lose their porosity over approximately 100 °C[23] and, at best, ~400 °C is the maximum.[24] Notably, the decomposition temperature of **CB3Ph6** crystal is over 500 °C as calculated from TGA curves (Table S2), which highlights material robustness owing to the inorganic 3D aromaticity of *o*-carborane scaffolds.[25,26] Moreover, in the variable-temperature PXRD measurement, the PXRD patterns of crystal was hardly changed at least up to 400 °C, indicating the superior heat resistance of porous crystal without decomposition and melting (Figure S12).

To evaluate the stability of crystal, the non-covalent interaction (NCI) plot[27] was made to visualize intra- and inter-column interaction in 1D **CB3Ph6** array formed in the crystal (Figure S13). In the NCI plot, vdW interactions existed between *o*-carborane units in crystal, while other interactions such as B–H···π and C–H···H–B were also visualized as indicated in the SCXRD data based on the interatomic

View Article Online
DOI: 10.1039/D5SC08753H

distances (Figures S1 and S2). Therefore, at this stage, these data suggest that multiple non-covalent interactions cooperatively contribute to the reinforcement of the porous structure and its thermal stability.

Furthermore, PXRD patterns ensured their high crystallinity as indicated by consistent peaks even after guest removal and refilling (Figure S4). These data suggest that rigid microporosity should be hardly affected by desorption and adsorption processes. Such high crystallinity enabled SCXRD analysis on **DBE@CB3Ph6** (Table S1, Figure S2). As we expected, **DBE@CB3Ph6** had the same crystalline packing to **DCE@CB3Ph6** except for the replacement of halogen atoms. Its space group was determined as *C*2/c, that is the same as **DCE@CB3Ph6** and **CB3Ph6**α. The differences in lattice constants between the two crystals were less than 1%. From these results, it can be concluded that the removal and re-uptake of vaporous guests proceed without crystal phase transition, amorphization and chemical decomposition (Figure 3c). The solid-gas adsorption experiment of **CB3Ph6**α with C_4H_{10} was also tested to investigate the guest selectivity. The adsorbed C_4H_{10} molecules were quantified by ^{1}H NMR measurements. After 30 min and 2 days of the adsorption experiment, the guest/host molar ratio was calculated as 0.49 and 0.13, respectively (Charts S8 and S9). With DCE, DBE, and BCE, 1:1 host–guest binding was maintained at least 30 min after the solid-vapor adsorption experiments (Charts S5–S7). These results indicate that **CB3Ph6**α can capture gaseous C_4H_{10}, while its host–guest binding with C_4H_{10} could be weaker than those with halogenated ethane derivatives. Thus, it is presumed that the halogen atoms might render the C–H bonds more electron-deficient, which in turn enhances the C–H···π interactions with the biphenyl units.

Optical properties

Optical measurements were conducted to understand the effect of macrocyclization and host–guest complexation in the crystalline state on excited-state relaxation processes. **CB3Ph6** showed only slight photoluminescence (PL) in the $CHCl_3$ solution (emission quantum yield (Φ_{PL}) < 0.01), while crystalline samples exhibited over 10 times larger values (Φ_{PL} > 0.10) (Tables 2 and S3). Moreover, **CB3Ph6** exhibited emission enhancement by aggregation in the THF/H_2O mixture, where THF and H_2O behaved as good and poor solvents, respectively (Figure S14). These results indicate that **CB3Ph6** is an AIEgen. Absorption spectra were hardly influenced by solvent polarity, whereas PL spectra were significantly

View Article Online
DOI: 10.1039/D5SC08753H

red-shifted as the polarity increased (Figure S15), meaning that the emission bands should be obtained from the ICT state in solution state. Crystalline samples showed structureless PL bands as observed in the solution state, indicating that the crystals should show ICT emission. From these results, it is suggested that in the excited state, macrocyclic **CB3Ph6** should have a significant relaxation pathway that is permissible even under structural constraints. Next, the effect of guest encapsulation was investigated with **CB3Ph6** crystals (Figure 4a, Table 2). The correspondence of the PXRD patterns between experimental and SCXRD simulated data (Figures S6 and S7) confirmed the phase purity of the solvated crystals. The guest-free crystal, **CB3Ph6**α, showed the PL band with maximum wavelength (λ_{PL}) at 461 nm and Φ_{PL} of 0.11. Host–guest complexation in the solvated crystals resulted in 14–23% increase of Φ_{PL} and 4–12 nm blue-shift of λ_{PL}. PL spectra of the solvated crystals were completely overlapped to each other, suggesting that luminescent properties should be obtained through similar mechanism despite uptaking different guests. Reversible guest encapsulation was also confirmed by the correspondence of PL spectra between **CB3Ph6**α exposed to DCE vapor (**DCE-fumed**) and **DCE@CB3Ph6** (Figure 4b) and re-enhanced Φ_{PL} value to 0.33 in **DCE-fumed**. To gather kinetic information, radiative and non-radiative constants (k_r and k_{nr}, respectively) were calculated by Φ_{PL} and lifetime data (Table 2, Figures S16 and S17. It was revealed that k_r values were hardly affected by solvent encapsulation, while k_{nr} values decreased by one order of magnitude. This result suggests that guest molecules should inhibit non-radiative decay processes. It is widely known that cryogenic temperature can suppress molecular motion that leads to non-radiative emission quenching. From **CB3Ph6** crystals, it was shown that cooling from room temperature to 77 K induced blue-shift of PL spectra by 15–17 nm (Figure S18) and significant emission enhancement regardless of the existence of guest solvents in the crystal packing (Figure S19). These cryogenic results corresponded to the phenomena observed upon solvent encapsulation, which further implies that included guest solvents should block molecular motions that cause emission quenching.

View Article Online
DOI: 10.1039/D5SC08753H

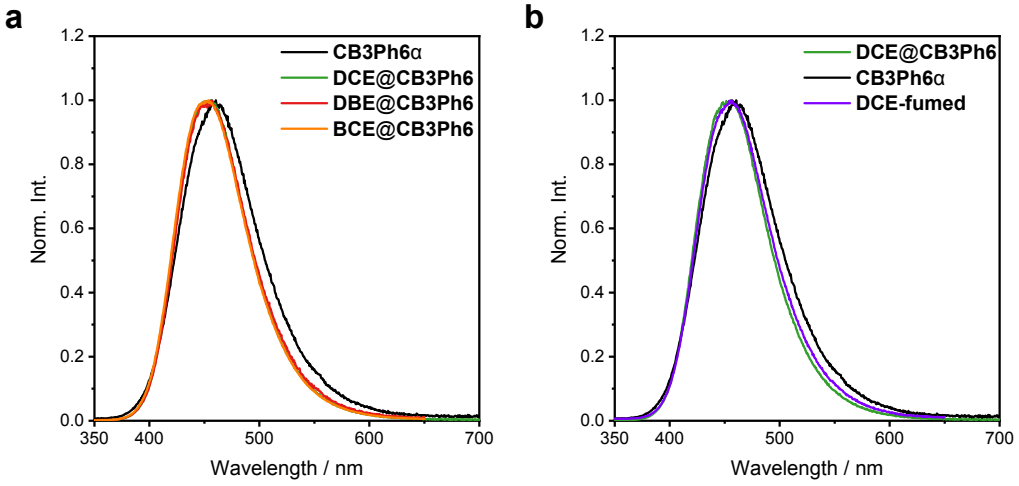

Figure 4. (a) PL spectra of **CB3Ph6α** (black), **DCE@CB3Ph6** (green), **DBE@CB3Ph6** (red), and **BCE@CB3Ph6** (orange). (b) PL spectra of **DCE@CB3Ph6** before (green) and after (**CB3Ph6α**, black) removal of vaporous guests and after re-uptake of DCE (**DCE-fumed**).

Table 2. Summary of solid-state optical properties

Crystal	λ_{PL} / nm[a]	Φ_{PL}[a,b]	τ_{PL} / ns[c]	τ_{PL}^{ave} / ns[d]	χ^2	k_r / ns^{-1}[e]	k_{nr} / ns^{-1}[f]
CB3Ph6α	461	0.11	2.8 (51%), 0.9 (38%), 0.07 (11%)	0.5	1.22	0.22	1.8
DCE@CB3Ph6	456	0.29	2.6 (17%), 1.5 (79%), 0.1 (4%)	1.1	1.06	0.26	0.65
DBE@CB3Ph6	457	0.25	2.6 (19%), 1.2 (76%), 0.1 (4%)	0.9	1.09	0.28	0.83
BCE@CB3Ph6	454	0.34	2.4 (14%), 1.3 (83%), 0.1 (3%)	1.1	0.99	0.28	0.63

[a] Excited at 276 nm. [b] Absolute quantum yield determined by the integrating sphere method. [c] Excited at 375 nm. [d] $\tau_{PL}^{ave} = \Sigma_i \tau_i f_i$, where f_i: relative amplitude of ith component (%), τ_i: luminescent decay lifetime of ith component(s). [e] $k_r = \Phi_{PL}/\tau_{PL}^{ave}$. [f] $k_{nr} = (1-\Phi_{PL})/\tau_{PL}^{ave}$.

DFT calculation

To discuss mechanism behind guest-induced emission enhancement, theoretical calculation was performed with density functional theory (DFT) and time-dependent DFT (TD-DFT). DFT calculations for the ground state show that the calculated structure is identical to the SCXRD structure (Figure 2a), and isolated **CB3Ph6** should have C_3-symmetry with equal length of the C_{cage}–C_{cage} bonds in three *o*-carborane units (1.75 Å) and vertically oriented biphenyl sides to the C_{cage}–C_{cage} bonds (Figures 5 left and S20a). Absorption transition (S_0 to S_1) contained molecular orbitals (MOs) contributed by biphenyl units (Figure S21). TD-DFT calculations for the excited state suggest a locally-stable geometry with the elongated C_{cage}–C_{cage} bond to 2.36 Å (Figures 5 middle and S20b). Emission transition (S_1 to S_0) is

View Article Online
DOI: 10.1039/D5SC08753H

calculated as ICT character between lowest unoccupied MO (LUMO) and highest occupied MO (HOMO). HOMO contains π* orbitals of two biphenyl units, while LUMO mainly extends on the *o*-carborane unit (Figure 5 middle). These results support that **CB3Ph6** exhibits ICT emission contributed by one *o*-carborane unit and two biphenyl units connected to it.

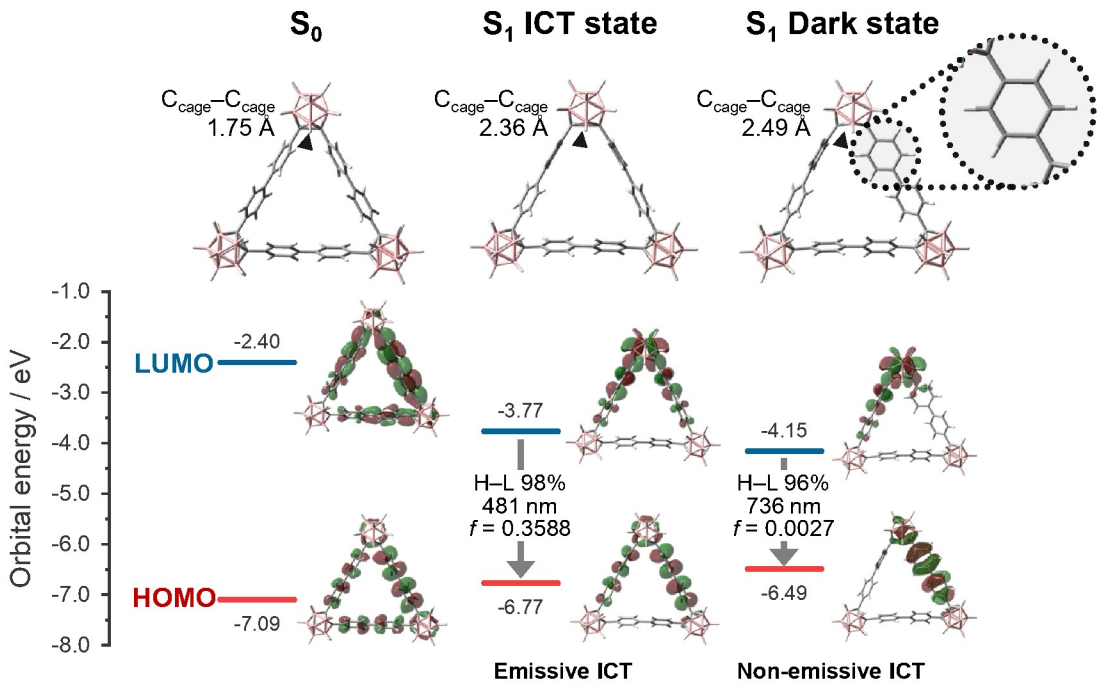

Figure 5. Optimized structures with C_{cage}–C_{cage} bond lengths and calculated Kohn–Sham frontier orbital distributions of S_0 (left), S_1 ICT (middle), and S_1 dark states (right) of **CB3Ph6** with electronic transition energy in nm and assigned emission characters for the S_1 states (colors: C, gray; B, pink; H, white). H–L indicates the proportion of HOMO–LUMO transitions consisting of $S_1 \rightarrow S_0$ transition. *f* denotes the oscillator strength. Isovalues are 0.02. B3LYP/6-31+G(d,p) was used. Red and blue bar plots indicate HOMO and LUMO energy levels, respectively.

To understand the guest-induced PL change, crystal-state calculation was performed with the quantum mechanics and molecular mechanics (QM/MM) method.[28] QM/MM calculation was modeled by cut out cluster of the SCXRD packing structures (Figure S22). The model structure for the guest-free crystal, **CB3Ph6**α, was prepared based on solvent-removed **DCE@CB3Ph6**. From the calculations, it was proposed that guest encapsulation of DCE and DBE can induce 4 and 6 nm blue shifts of PL spectra,

View Article Online
DOI: 10.1039/D5SC08753H

respectively, and these results are in close agreement with experimental data, where blue shifts up to 7 nm were observed (Table S4). In addition, guest encapsulation slightly suppressed C_{cage}–C_{cage} bond elongation (Figures S23a–c). It is implied that structural relaxation in the excited state followed by PL blue shift might be caused by the limited structural relaxation. Furthermore, in the non-emissive dark excited states, the distributions of HOMO and LUMO were almost separated (Figure 5 right). As a result, the corresponding emission transitions are forbidden with almost no oscillator strength due to the only slight overlap between HOMO and LUMO distributions (Table S17). In the dark state, isolated **CB3Ph6** had the C_{cage}–C_{cage} bond of 2.49 Å and parallel orientation of one biphenyl unit to the elongated bond (Figures 5 right and S20c). The rotated biphenyl moiety partially filled internal cavities of **CB3Ph6**. The crystalline dark states were also found from the calculations with the QM/MM method (Figures S23d–f). The dark state of **CB3Ph6**α was destabilized by 0.19 eV as compared to the corresponding ICT state. Significantly, the degree of destabilization was enlarged by guest encapsulation; energy levels of the dark states of DCE and DBE in crystal should be 0.38 and 0.44 eV higher than those of their ICT states, respectively (Table S5). In other system, it has been reported that guest-induced PL changes are related to the suppression of structural changes in the excited state.[29] In this case, experimentally observed guest-induced emission enhancement of **CB3Ph6** was associated with the decreased non-radiative decay constants possibly due to the suppression of excited-state structural relaxation. Assuming ultrafast decay in the dark state, these results suggest a possibility that, without guest-loading, benzene rings can rotate in cavity smoothly, that accelerate relaxation to non-emissive dark state, while guest filling could partially disturb the formation of dark states via steric repulsion. Then it should facilitate trapping more excitons in the emissive ICT states. Finally, emission enhancements could be induced by guest encapsulation (Figure 6).

View Article Online
DOI: 10.1039/D5SC08753H

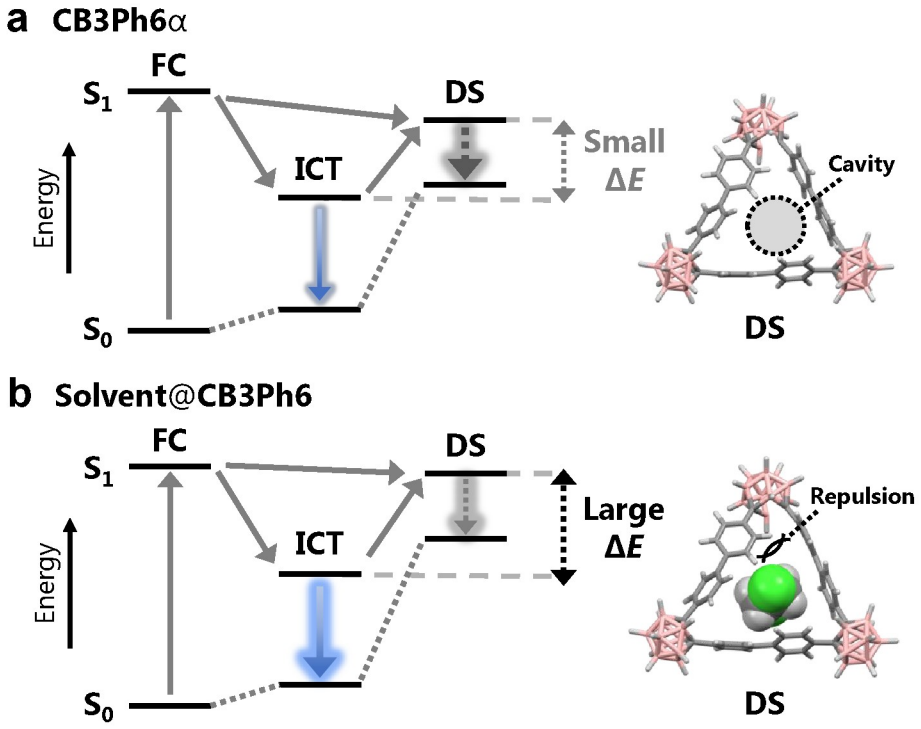

Figure 6. Schematic illustration on the energy diagrams of a) **CB3Ph6**α and b) Guest encapsulated **CB3Ph6** crystals with the corresponding QM calculated molecular structure of dark states (Colors: C, gray; B, pink; H, white; Cl, green), in which solvent represents DCE, DBE, and BCE. FC, ICT, and DS denote Franck–Condon, intramolecular charge transfer, and dark states, respectively. Blue solid and gray dotted arrows indicate transitions dominated by radiative and non-radiative decays, respectively.

Conclusion

In conclusion, we have shown that **CB3Ph6**, a novel AIE-active *o*-carborane-based macrocycle, can form permanent intrinsic porous crystal with 1D channels. Solid-vapor adsorption indicated that vaporous halogenated ethane derivatives can thread into the channel to construct 1:1 host–guest complex. The crystal can be processed with reversible guest removal and encapsulation without losing its porosity and crystallinity. Vapor inclusion induced blue-shift and enhancement of PL efficiency. Theoretical calculation data suggest that cavity-filling by vaporous guests could restrict excited-state structural relaxation in the crystal state. Furthermore, the porous crystal has excellent thermal stability up to 500 °C. One possible application of our material is the separation and detection of alkane and alkyne, based on whether multiple effective C–H···π interactions can be formed. Our finding might contribute to expanding design and application of smart materials based on porous molecular crystals utilizing AIEgens.

View Article Online
DOI: 10.1039/D5SC08753H

Data availability

The data supporting this article have been included as part of the ESI.† Crystallographic data for **DCE@CB3Ph6** and **DBE@CB3Ph6** have been deposited at the CCDC under 2495493 and 2495494.

Author contributions

K. Y., S. T., T. Y., and S. O. performed experiments and conducted data analysis. K. Y. conducted investigation and wrote the original draft. K. Y. and K. T. conceptualized the research framework. T. O. and K. T. provided resources and supervised the project. All authors discussed the results and contributed to reviewing and editing the manuscript.

Conflicts of interest

There are no conflicts to declare.

Acknowledgements

This work was partially supported by a Grant-in-Aid for Scientific Research (B) (for K.T., JSPS KAKENHI Grant Number, 24K01570) and the National Research Foundation of Korea (NRF) grant funded by the Korea government (MSIT) (No. RS-2024-00406152).

Reference

1 M. K. Bera, P. Pal and S. Malik, Solid-state emissive organic chromophores: Design, strategy and building blocks, *J. Mater. Chem. C*, 2020, **8**, 788–802.

2 J. Mei, Y. Hong, J. W. Y. Lam, A. Qin, Y. Tang and B. Z. Tang, Aggregation-induced emission: The whole is more brilliant than the parts, *Adv. Mater.*, 2014, **26**, 5429–5479.

3 Y. Cai, L. Du, K. Samedov, X. Gu, F. Qi, H. H. Y. Sung, B. O. Patrick, Z. Yan, X. Jiang, H. Zhang, J. W. Y. Lam, I. D. Williams, D. Lee Phillips, A. Qin and B. Z. Tang, Deciphering the working mechanism of aggregation-induced emission of tetraphenylethylene derivatives by ultrafast spectroscopy, *Chem. Sci.*, 2018, **9**, 4662–4670.

4 Y. Fujimoto, Y. Mochiduki, H. Sotome, R. Shimada, H. Okajima, Y. Toda, A. Sakamoto, H. Miyasaka and F. Ito, Excited State Dynamics of Geometrical Evolution of α-Substituted Dibenzoylmethanatoboron Difluoride Complex with Aggregation-Induced Emission Property, *J. Am. Chem. Soc.*, 2024, **146**, 32529–32538.

5 Z. Jianyu, Z. Haoke, L. W. Jacky Y and T. Ben Zhong, Restriction of Intramolecular Motion(RIM): Investigating AIE Mechanism from Experimental and Theoretical Studies, *Chem. Res. Chin. Univ.*, 2021, **2021**, 1–15.

6 Y. Duo, L. Han, Y. Yang, Z. Wang, L. Wang, J. Chen, Z. Xiang, J. Yoon, G. Luo and B. Z. Tang, Aggregation-Induced Emission Luminogen: Role in Biopsy for Precision Medicine, *Chem. Rev.*, 2024, **124**, 11242–11347.

View Article Online
DOI: 10.1039/D5SC08753H

7 Y. Huang, L. Ning, X. Zhang, Q. Zhou, Q. Gong and Q. Zhang, Stimuli-fluorochromic smart organic materials, *Chem. Soc. Rev.*, 2024, **53**, 1090–1166.

8 K. Imato and Y. Ooyama, Stimuli-responsive smart polymers based on functional dyes, *Polym. J.*, 2024, **56**, 1093–1109.

9 J. R. Wu, G. Wu, D. Li and Y. W. Yang, Macrocycle-Based Crystalline Supramolecular Assemblies Built with Intermolecular Charge-Transfer Interactions, *Angew. Chem. Int. Ed.*, 2023, **62**, e202218142.

10 A. Liu and Y. W. Yang, Aggregation-induced emission in synthetic macrocycle-based supramolecular systems, *Chem. Commun.*, 2025, **61**, 13827–13840.

11 J. Ochi, K. Tanaka and Y. Chujo, Recent Progress in the Development of Solid-State Luminescent o-Carboranes with Stimuli Responsivity, *Angew. Chem. Int. Ed.*, 2020, **59**, 9841–9855.

12 L. A. Boyd, W. Clegg, R. C. B. Copley, M. G. Davidson, M. A. Fox, T. G. Hibbert, J. A. K. Howard, A. Mackinnon, R. J. Peace and K. Wade, Exo-π-bonding to an ortho-carborane hypercarbon atom: Systematic icosahedral cage distortions reflected in the structures of the fluoro-, hydroxy- and amino-carboranes, 1-X-2-Ph-1,2-C2B10H 10 (X = F, OH or NH2) and related anions, *Dalton Trans.*, 2004, 2786–2799.

13 H. Naito, K. Nishino, Y. Morisaki, K. Tanaka and Y. Chujo, Solid-State Emission of the Anthracene-o-Carborane Dyad from the Twisted-Intramolecular Charge Transfer in the Crystalline State, *Angew. Chem. Int. Ed.*, 2017, **56**, 254–259.

14 D. Tahaoğ Lu, H. Usta and F. Alkan, Revisiting the Role of Charge Transfer in the Emission Properties of Carborane−Fluorophore Systems: A TDDFT Investigation, *J. Phys. Chem. A*, 2022, **126**, 4199–4210.

15 L. Ji, S. Riese, A. Schmiedel, M. Holzapfel, M. Fest, J. Nitsch, B. F. E. Curchod, A. Friedrich, L. Wu, H. H. Al Mamari, S. Hammer, J. Pflaum, M. A. Fox, D. J. Tozer, M. Finze, C. Lambert and T. B. Marder, Thermodynamic equilibrium between locally excited and charge-transfer states through thermally activated charge transfer in 1-(pyren-2′-yl)-o-carborane, *Chem. Sci.*, 2022, **13**, 5205–5219.

16 M. Tokutomi, K. Yuhara and K. Tanaka, Macrocyclic C,C′-diaryl-o-carborane derivatives containing pseudo-crown ether: emission enhancement upon cation recognition, *Phys. Chem. Chem. Phys.*, 2025, **27**, 15845–15849.

17 Y. Wang, H. Wu and J. F. Stoddart, Molecular Triangles: A New Class of Macrocycles, *Acc. Chem. Res.*, 2021, **54**, 2027–2039.

18 A. Chaix, G. Mouchaham, A. Shkurenko, P. Hoang, B. Moosa, P. M. Bhatt, K. Adil, K. N. Salama, M. Eddaoudi and N. M. Khashab, Trianglamine-Based Supramolecular Organic Framework with Permanent Intrinsic Porosity and Tunable Selectivity, *J. Am. Chem. Soc.*, 2018, **140**, 14571–14575.

19 Q. Qu, M. Fu, C. Lin, Y. Geng, Y. Li and Y. Yuan, Synthesis, properties and application of o-carborane-based π-conjugated macrocycles, *Org. Chem. Front.*, 2023, **10**, 3293–3299.

20 W. Jiang, I. T. Chizhevsky, M. D. Mortimer, W. Chen, C. B. Knobler, S. E. Johnson, F. A. Gomez and M. F. Hawthorne, Carboracycles: Macrocyclic Compounds Composed of Carborane Icosahedra Linked by Organic Bridging Groups, *Inorg. Chem.*, 1996, **35**, 5417–5426.

View Article Online
DOI: 10.1039/D5SC08753H

21 M. Mastalerz, Permanent porous materials from discrete organic molecules-towards ultra-high surface areas, *Chem. Eur. J.*, 2012, **18**, 10082–10091.

22 S. Cheng, L. Zong, K. Yuan, J. Han, X. Jian and J. Wang, Synthesis and thermal properties of an acetylenic monomer containing boron and silicon, *RSC Adv.*, 2016, **6**, 88403–88410.

23 H. Yamagishi, Functions and fundamentals of porous molecular crystals sustained by labile bonds, *Chem. Commun.*, 2022, **58**, 11887–11897.

24 C. G. Bezzu, L. A. Burt, C. J. McMonagle, S. A. Moggach, B. M. Kariuki, D. R. Allan, M. Warren and N. B. McKeown, Highly stable fullerene-based porous molecular crystals with open metal sites, *Nat. Mater.*, 2019, **18**, 740–745.

25 A. Muñoz-Castro, Aromatic trails: persistence and interplay between linked spherical aromatic dicarboranes in dimer to hexamer linear arrays, *Phys. Chem. Chem. Phys.*, 2025, **27**, 5249–5255.

26 P. L. Rodríguez-Kessler and A. Muñoz-Castro, Macrocyclic meta-carborane hexamer. Evaluation of aromatic characteristics as a cluster-based analog to phenyl-bridged macrocyclic structures, *Phys. Chem. Chem. Phys.*, 2025, **27**, 6744–6750.

27 E. R. Johnson, S. Keinan, P. Mori-Sánchez, J. Contreras-García, A. J. Cohen and W. Yang, Revealing noncovalent interactions, *J. Am. Chem. Soc.*, 2010, **132**, 6498–6506.

28 Q. Wu, T. Zhang, Q. Peng, D. Wang and Z. Shuai, Aggregation induced blue-shifted emission-the molecular picture from a QM/MM study, *Phys. Chem. Chem. Phys.*, 2014, **16**, 5545–5552.

29 M. Rojas-Poblete, P. L. Rodríguez-Kessler, R. Guajardo Maturana and A. Muñoz-Castro, Coinage-metal pillarplexes hosts. Insights into host-guest interaction nature and luminescence quenching effects, *Phys. Chem. Chem. Phys.*, 2021, **23**, 15917–15924.

View Article Online
DOI: 10.1039/D5SC08753H

The data supporting this article have been included as part of the Supplementary Information. Crystallographic data for **DCE@CB3Ph6** and **DBE@CB3Ph6** has been deposited at the CCDC under 2495493 and 2495494.